J Geod (2007) 81:311–323
DOI 10.1007/s00190-006-0114-0

ORIGINAL ARTICLE

Temporal correlations of atmospheric mapping function errors in GPS estimation

Borys Stoew · Tobias Nilsson · Gunnar Elgered · Per O. J. Jarlemark

Received: 12 July 2005 / Accepted: 4 October 2006 / Published online: 2 December 2006

Abstract The developments in global satellite navigation using GPS, GLONASS, and Galileo will yield more observations at various elevation angles. The inclusion of data acquired at low elevation angles allows for geometrically stronger solutions. The vertical coordinate estimate of a GPS site is one of the parameters affected by the elevation-dependent error sources, especially the atmospheric corrections, whose proper description becomes necessary. In this work, we derive time-series of normalized propagation delays in the neutral atmosphere using ray tracing of radiosonde data, and compare these to the widely used new mapping functions (NMF) and improved mapping functions (IMF). Performance analysis of mapping functions is carried out in terms of bias and uncertainty introduced in the vertical coordinate. Simulation runs show that time-correlated mapping errors introduce vertical coordinate RMS errors as large as 4 mm for an elevation cut-off angle of 5°. When simulation results are compared with a geodetic GPS solution, the variations in the vertical coordinate due to mapping errors for an elevation cut-off of 5° are similar in magnitude to those caused by all error sources combined at 15° cut-off. This is significant for the calculation of the error budget in geodetic GPS applications. The results presented here are valid for a limited area in North Europe, but the technique is applicable to any region provided that radiosonde data are available.

Keywords Mapping functions · Elevation cut-off · Vertical component errors · Error correlations · Atmospheric refraction · Geodetic GPS

B. Stoew (✉) · T. Nilsson · G. Elgered
Department of Radio and Space Science,
Chalmers University of Technology,
Onsala Space Observatory, 43 992 Onsala, Sweden
e-mail: boris@oso.chalmers.se

T. Nilsson
e-mail: tobias@oso.chalmers.se

G. Elgered
e-mail: kge@oso.chalmers.se

P. O. J. Jarlemark
Swedish National Testing and Research Institute,
Box 857, 501 15 Borås, Sweden
e-mail: Per.Jarlemark@sp.se

1 Introduction

The statistical description of estimation errors is important both for geodetic and meteorological applications using ground-based GPS networks. The temporal correlations of these errors influence the trends in the measured land uplift (e.g., Scherneck et al. 2003). These correlations also need to be described for the eventual assimilation of the zenith total delay (ZTD) estimates into a numerical weather prediction (NWP) model, particularly for the weighting of past data in an observation bias reduction scheme (Daley 1992).

The atmospheric delay errors and the vertical station position errors are closely related, having common sources, such as the satellite orbit and clock errors, and inaccuracies in the used models of the neutral atmosphere (e.g., Jarlemark et al. 2001). The present study will help to better evaluate the error budget for geodetic GPS data processing, as well as weather forecasting and real-time applications.

In space-geodetic applications, the atmospheric delay is traditionally modeled as a composition of two parts: the first being the ZTD, and the second mapping the ZTD to the slant delay in the direction of the observations (Herring et al. 1990). In order to utilize the inherent positioning accuracy in the GPS technique, it is necessary to work separately with the hydrostatic and the wet delays using an optimized mapping function (MF) for each component. A number of MF formulas have been proposed taking into account parameters that are easily accessible, such as surface meteorological observations, day of the year, and the site altitude (Davis et al. 1985; Ifadis 1986; Herring 1992).

The MFs have been further developed by Niell (1996, 2000, 2001). The performance of the commonly used new and improved MFs (NMF and IMF) is comparable with, or better than, that of the previously used ones. The NMFs are practical since no in situ acquisition of meteorological data is required for their use. The parameterization of the NMFs is based on statistics obtained from ray-traced radiosonde measurements. MFs using data from NWP models have also been introduced (Rocken et al. 2001; Niell et al. 2001).

In this article, we address the influence of the MF errors on the vertical coordinate and atmospheric delay estimates. This is carried out using both simulations and real data from a GPS receiver network in Sweden. The results apply to a common geodetic processing strategy, and assume a horizontally isotropic troposphere. Methods for estimating 2D atmospheric delay gradients exist (e.g., Davis et al. 1993; Bar-Sever et al. 1998). However, simultaneous radiosonde launches from the same location are very rare, and do not provide useful data for the analysis of MF errors in the anisotropic case.

In Sect. 2, we discuss the radiosonde data used in a ray-tracing algorithm to deduce the propagation delay residuals for a given MF. We also review the atmospheric delay MFs considered in this study. In Sect. 3, we present the means and the standard deviations of the MF residuals at different elevation angles. Section 4 introduces the elevation-dependent models for the means and standard deviations of the MF errors, and a Gauss–Markov model describing their statistical behavior.

In Sect. 5, we show simulation results and investigate the effect of the chosen MFs on the vertical coordinate estimates. Section 6 presents time-series of GPS vertical position residuals from a local geodetic receiver network, and discusses the relation between the zenith delay estimation errors and the height residuals, putting in perspective the choice of elevation cut-off angle. We also discuss the time correlations of the GPS atmospheric delay estimation errors obtained using water vapor radiometer (WVR) data. The conclusions follow in Sect. 7.

2 Ray tracing using meteorological data

2.1 Radiosonde data as a base for comparison

Balloon-borne sensors can be used to acquire vertical profiles of temperature, pressure, humidity, and wind. The data obtained from these atmosphere soundings are often reduced to profiles containing the values at a set of standard pressure levels, along with the levels representing significant changes in the observed atmospheric parameters. These parameters relate to the refractivity (e.g., Crane 1976; Davis et al. 1985):

$$\begin{aligned} N &= k_1 \frac{p_\mathrm{d}}{T} + k_2 \frac{e}{T} + k_3 \frac{e}{T^2} \\ &= k_1 \frac{p_\mathrm{t}}{T} + (k_2 - k_1) \frac{e}{T} + k_3 \frac{e}{T^2} \end{aligned} \tag{1}$$

where the parameters k_1, k_2, and k_3 are empirically determined from laboratory experiments; p_d represents the sum of the partial pressures of the "dry" gases, e is the partial pressure of water vapor, p_t is the total pressure, and T is the absolute temperature of the air parcel.

The refractivity can be split into a hydrostatic (dry) and a non-hydrostatic (wet) part (Davis et al. 1985). The integration of these refractivities produces the respective propagation path delays in the neutral atmosphere, which are then used as the base for the MF error comparisons. The hydrostatic delay can be derived accurately from ground pressure observations (ibid.), whereas the wet term requires actual profiles of meteorological data.

2.2 Hydrostatic and wet mapping functions

The GPS carrier-phase observation is usually expressed in units of length as:

$$\Phi = \rho + c\,(\tau_\mathrm{sat} - \tau_\mathrm{rec}) - \ell_\mathrm{ion} + \ell + \lambda M + \nu_\Phi\,, \tag{2}$$

where ρ is the geometric distance from the receiver to the satellite, c is the speed of light, τ_sat and τ_rec are the clock biases at the transmitter and the receiver, respectively, λ is the wavelength of the carrier wave considered, and M is an integer describing the carrier-phase ambiguity. The estimation errors are typically caused by the satellite and receiver clock drifts, the ionospheric delay ℓ_ion, the neutral atmospheric delay ℓ, and satellite orbit errors. Finally, ν_Φ represents the unmodeled phase measurement errors, such as atmospheric modeling errors, multipath interference, and errors related to the used antenna radiation pattern model.

The slant hydrostatic/wet propagation delay is usually converted to the respective *equivalent* zenith delay using MFs. As an example, the hydrostatic mapping function (MFh) $m_h(\varepsilon)$ relates the equivalent zenith hydrostatic delay $\ell_h^z(\varepsilon)$ to the slant hydrostatic delay $\ell_h(\varepsilon)$:

$$\ell_h(\varepsilon) = \ell_h^z(\varepsilon)\, m_h(\varepsilon)\,, \tag{3}$$

where ε is the satellite elevation angle.

The estimate of the zenith hydrostatic delay ℓ_h^z (hereafter ZHD) is a weighted average of the equivalent zenith delays $\ell_h^z(\varepsilon_i)$, calculated using data for the directions toward the satellites visible at a given epoch. The ZHD differs from the actual value of the delay in the zenith direction, $\ell_h(90°)$, due to (a) heterogeneities of the atmosphere, and (b) imperfections in the MF used. The wet MF (MFw) and the slant/zenith wet delays are related in a way similar to Eq. (3).

Assuming that the atmosphere is stratified and horizontally isotropic above the GPS receiver, the total slant delay estimates can be expressed as

$$\ell(\varepsilon) = \ell_h^z\, m_h(\varepsilon) + \ell_w^z\, m_w(\varepsilon)\,, \tag{4}$$

where ℓ_w^z denotes the zenith wet delay (ZWD) estimate. In a typical setup of geodetic data-analysis software, ℓ_h^z is either modeled or computed from ground observations; ℓ_w^z is estimated assuming it has random walk properties (Johansson et al. 2002). It has been recognized that the weakest assumptions in such an arrangement relate to the utilized MFs (Herring et al. 1990). The MFs currently used in GPS data processing introduce a root-mean-square (RMS) error of less than 6 mm in the ZTD for $\varepsilon > 10°$ (Bisnath et al. 1997; Niell 1996).

The Ifadis (1986) global MFs are applicable for $\varepsilon > 2°$, and utilize surface measurements of the temperature, water vapor partial pressure and total pressure. The Ifadis MFs are defined as:

$$m(\varepsilon) = \frac{1}{\sin\varepsilon + \dfrac{a}{\sin\varepsilon + \dfrac{b}{\sin\varepsilon + c}}}\,, \tag{5}$$

where the values of a, b, and c are different for the dry and the wet part, and are obtained using meteorological data acquired at the desired location (Ifadis 1986).

The hydrostatic and wet NMFs (NMFh and NMFw) are based on statistics covering radiosonde ascents from 26 locations worldwide (Niell 1996). The parameters of NMFw depend only on site latitude, while the behavior of the NMFh depends also on the day of the year and the station height. These MFs have been derived for elevation angles $\varepsilon > 3°$, and have the general form:

$$m(\varepsilon) = \frac{1 + \dfrac{a}{1 + \dfrac{b}{1+c}}}{\sin\varepsilon + \dfrac{a}{\sin\varepsilon + \dfrac{b}{\sin\varepsilon + c}}}\,, \tag{6}$$

where the parameters a, b, and c are obtained from models using information about the site location and day of the year. For a detailed discussion of these parameters and their derivation, we refer to the original work by Niell (1996).

Figure 1 shows time-series of the NMFh and the Ifadis MFh values for $\varepsilon = 10°$ for the radiosonde launch site at the Gothenburg Landvetter Airport, Sweden (57.67°N, 12.30°E, 164 m above sea level, hereafter referred to as Landvetter). The largest systematic differences between these two MFs are in the winter and reach only 0.1% for this site. The short-term variations in the Ifadis MF are due to the behavior of the atmospheric parameters used in the calculation of the MF values. Note that at smaller elevation angles, the absolute MF values increase, reflecting that the portion of the propagation path through the troposphere is larger. At lower latitudes, the MF values tend to decrease since the troposphere becomes thicker, which, together with the Earth's curvature, changes the relative contribution of the refractivity from high altitudes.

The IMFs are defined using Eq. (6). Their parameterization is based on meteorological data provided by an NWP model, normally available at six-hourly intervals on a global 3D grid (Niell 2001, 2003). The hydrostatic

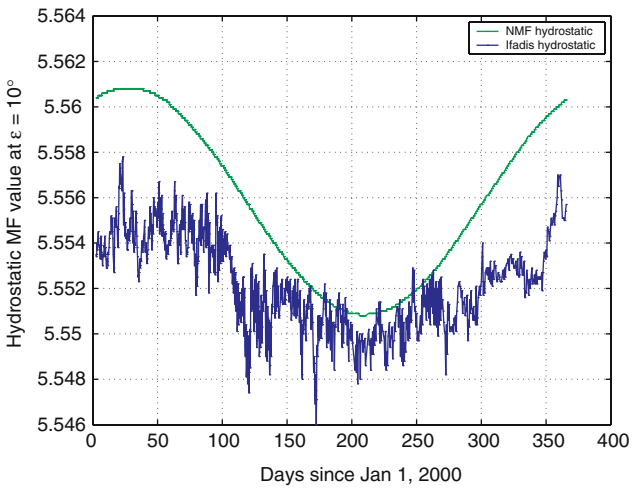

Fig. 1 Time-series of the NMFh and Ifadis MFh, calculated for $\varepsilon = 10°$ at Landvetter, Sweden. The seasonal variations in the NMFh depend only on the latitude of the site and the day of the year, while the Ifadis MFh utilizes surface measurements

IMF (IMFh) uses the height of the 200 hPa pressure level and the site coordinates. The wet IMF (IMFw) uses vertical profiles of temperature, pressure, and relative humidity, obtained using radiosondes or an NWP model. Both IMFs should be used for $\varepsilon > 3°$.

2.3 MF residuals derived using ray tracing

We utilized the same ray-tracing procedure that was used for deriving the NMFs (Niell 1996). It assumes a horizontally isotropic atmosphere above the radiosonde launch site. This procedure integrates vertical profiles of relative humidity, air temperature, and pressure in order to obtain the wet and hydrostatic propagation delays, and the geometric delays for a given elevation angle.

The results from the ray-tracing procedure include the normalized wet/hydrostatic atmosphere thickness (slant delays divided by the corresponding zenith delays), which represents the true value of the MF. The normalized thickness is then directly compared with the Ifadis MF, NMF, and IMF values, in order to derive the MF residuals for $\varepsilon = \{3, 5, 7, 10, 15, 20, 30, 45, 60\}°$. The values of ε are chosen at irregular intervals, reflecting the increased sensitivity of the MF parameters at low elevation angles.

Ideally, the time correlations of the MF residuals should represent the behavior of the GPS slant delay estimation errors for a given ε. Time-series of slant delay residuals due to the Ifadis MFh/MFw are shown in Fig. 2 for Landvetter.

Note the slowly varying offset in the slant hydrostatic delay (the Ifadis MFh underestimates the ray-trace results in the winter). This offset causes the correlations of the Ifadis MFh residual to be rather high on weekly time scales. The variations of the Ifadis MFh are six times larger than those of the MFw, meaning that the combined errors due to the Ifadis MFs have long correlation times. Furthermore, there is an apparent diurnal signature in these correlations, which should be attributed to the differences between the day-time and night-time variations of the temperature profile (Niell 1996).

The slant delay residuals due to the NMFs, and the temporal correlations of the NMFh/NMFw residuals are shown in Fig. 3, spanning the year 2000. Note that for the NMFw, the residuals appear uncorrelated on scales longer than 1 day, while the MFh residuals are correlated on scales of several days.

We generated the IMFs for a fictitious GPS receiver at Landvetter, using meteorological data from this radiosonde site. In practice, very few GPS and radiosonde stations are co-located, the radiosonde launches are costly, suggesting that NWP data can be used instead. However,

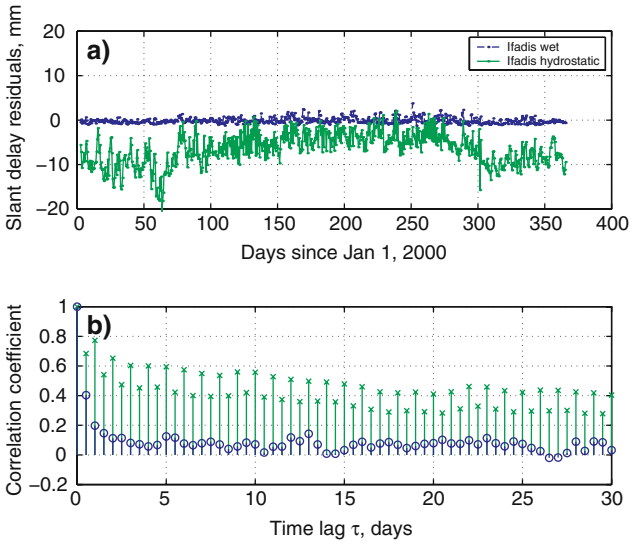

Fig. 2 **a** Slant delay residuals for the Ifadis MFs, calculated for $\varepsilon = 10°$ using semi-daily radiosonde data acquired at Landvetter (year 2000). The RMS variations of the Ifadis MFh residuals are about six times larger than those of the MFw; there is also a systematic offset in the MFh for this site. **b** Temporal correlations of the Ifadis MF residuals: the Ifadis MFw residuals (*circle*) are uncorrelated for time-scales larger than 1 day; the Ifadis MFh residuals (*cross*) are correlated on scales of several days and exhibit a diurnal pattern

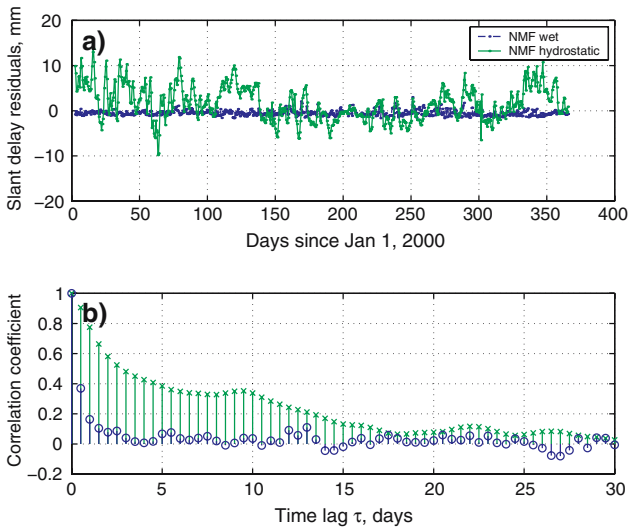

Fig. 3 **a** Slant delay residuals for the NMFs, calculated for $\varepsilon = 10°$ for Landvetter (year 2000). The RMS variations of the NMFh residuals are about five times larger than those of the NMFw. **b** Temporal correlations of the NMF residuals: the NMFw residuals (*circle*) are practically uncorrelated on scales larger than 1 day, while the NMFh residuals (*cross*) are correlated on scales of several days

the NWP model itself will introduce time-correlated estimation errors, which are difficult to quantify.

Figure 4 presents time-series of the slant delay residuals due to the IMFh/IMFw, together with the corresponding time-correlation sequences for the year 2000.

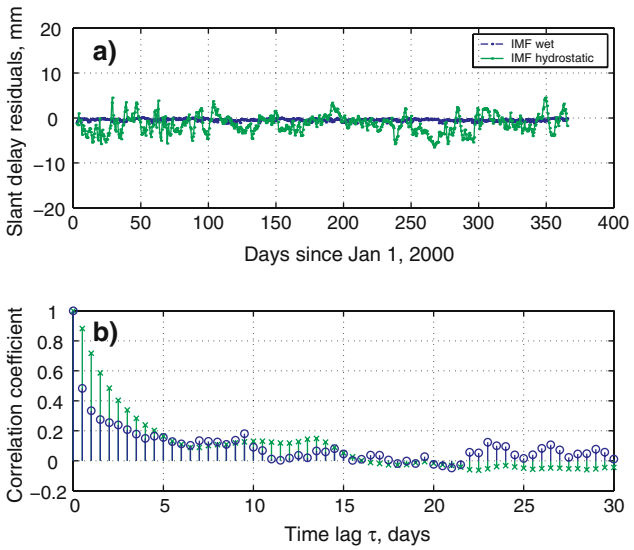

Fig. 4 **a** Slant delay residuals for the IMFs, calculated for $\varepsilon = 10°$ at Landvetter. The variations of the IMFh residuals are about two times smaller compared with those of the NMFh (Fig. 3a). **b** Temporal correlations of the IMF residuals: both the IMFw residuals (*circle*) and the IMFh residuals (*cross*) are correlated on scales of several days

The time correlations of the IMFh residuals suggest smaller systematic errors, which is likely due to the use of in situ measurements in the parameterization. The variability of the slant delay residuals due to the IMFs is smaller compared to the NMF case, as demonstrated by Figs. 5 and 6.

The values of the temporal correlations of the residuals of all three MFs change insignificantly (only by about 1%) when the different elevation angles are considered. Note that when shorter periods of time are processed, the slowly varying offset in the MF errors has a smaller impact on the calculated time correlations, and the errors appear to have shorter decorrelation times.

Since the atmospheric variations affect the estimated geodetic parameters, particularly the station height, relating the estimation errors to these variations is worthwhile (Herring et al. 1990). Geodetic position solutions become stronger if the low-elevation observations are included because the geometry is improved. However, such an improvement is difficult to realize if the slant atmospheric delays are improperly modeled.

3 Description of the MF errors

A change in the elevation cut-off angle for the data included in a GPS solution introduces an offset in the vertical coordinate estimate of the site position as a consequence of the errors in the MFs used (e.g., Niell 1996; MacMillan and Ma 1994). The changes in the solution geometry, the antenna phase pattern, or the multipath effects are not taken into account here, since they are considered repetitive for a given cut-off angle in our simulation study.

In this section, we will focus on the characterization of the errors caused by the commonly used NMFh/NMFw and the newer IMFh/IMFw. We assume azimuthal symmetry of the atmospheric conditions above the considered location, as we derive the MF error statistics using radiosonde data. It becomes possible to model the slant delay errors using the information contained in these errors' elevation-dependent mean and standard deviation.

3.1 NMF residuals

The residual slant delays based on radiosonde ray tracing show a very good correlation for the different elevation angles. Figure 5 presents a correlation plot for the residuals at the elevations 3° and 10°. For $\varepsilon = 3°$, the slant delay errors due to the use of the NMFh reach up to 0.2 m. The correlation coefficients for the residual time-series for all pairs of low elevation angles were about 0.99. These high correlation values are due to

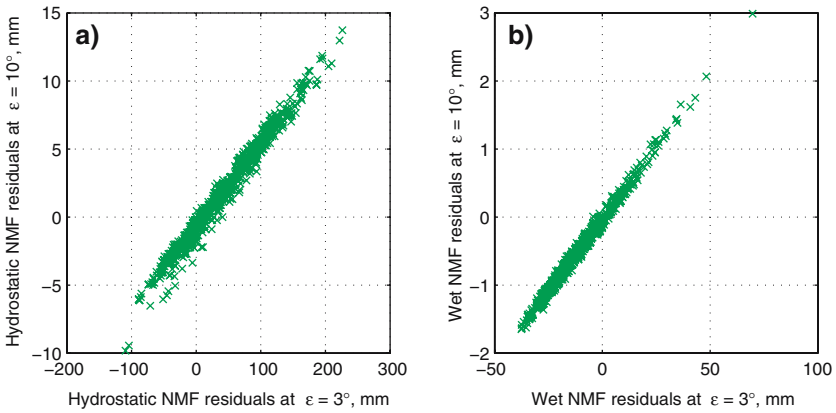

Fig. 5 Scatter plots for the slant delay residuals of the NMFs, calculated for $\varepsilon = \{3°, 10°\}$ at Landvetter (year 2000). **a** The slant delay residuals due to the NMFh have a positive offset; **b** the residuals due to the NMFw have a negative offset for this site

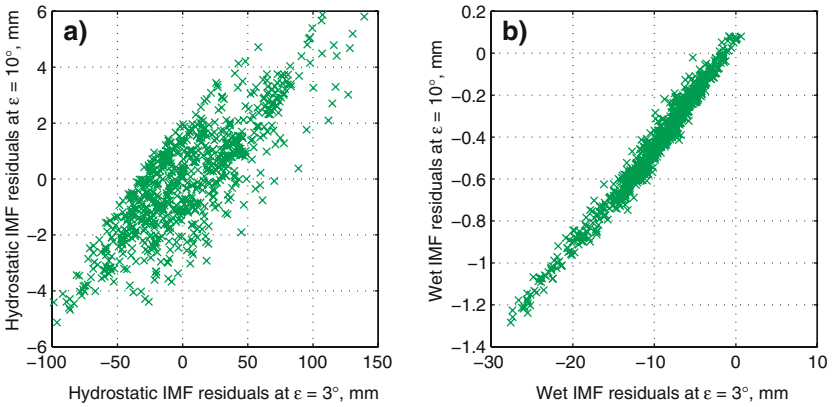

Fig. 6 Scatter plots for the slant delay residuals for the hydrostatic and wet IMFs, calculated for $\varepsilon = \{3°, 10°\}$ at Landvetter (year 2000). **a** The offset due to the IMFh is almost eliminated compared to the NMFh case; **b** the IMFw causes an elevation-dependent negative offset

the assumption that the radiosonde profiles represent a stratified atmosphere, and neglect all horizontal heterogeneities.

The apparent positive offset of the slant delay residuals due to the NMFh is elevation dependent (shown in Fig. 7), and causes an underestimation of the ZHD when low-elevation GPS measurements are used. The slant delay residuals due to the NMFw have a negative offset, leading to an overestimation of the ZWD. Both offsets are due to imperfections of the global model for the NMFs, and can be corrected using a site-specific exponential function of the elevation angle, as will be shown in Sect. 4.

The impact of these offsets is quantified using simulations at different elevation cut-off angles in Sect. 5. The NMF offsets are likely due to the fact that Scandinavia has a warmer climate compared with other regions at the same latitude. The MF biases, related to the local conditions, can be reduced with the use of radiosonde data for the parameterization of the IMFs.

The standard deviations of the slant delay residuals for a given elevation angle are presented in Fig. 8. Note that the variability of the residuals becomes significant at low elevations, and in Sect. 4 we introduce a model describing this dependence.

3.2 IMF residuals

The IMF parameters were obtained analyzing the same radiosonde data that provided the ray-traced slant delays. Thus, the scatter plot in Fig. 6 shows a reduced spread of the IMF residuals. Note that the correlation coefficient for the IMFh errors in Fig. 6 is about 0.80, and the offsets and the variations of the IMFh residuals are smaller compared with those of the NMFh (as seen in Figs. 5a, 7a).

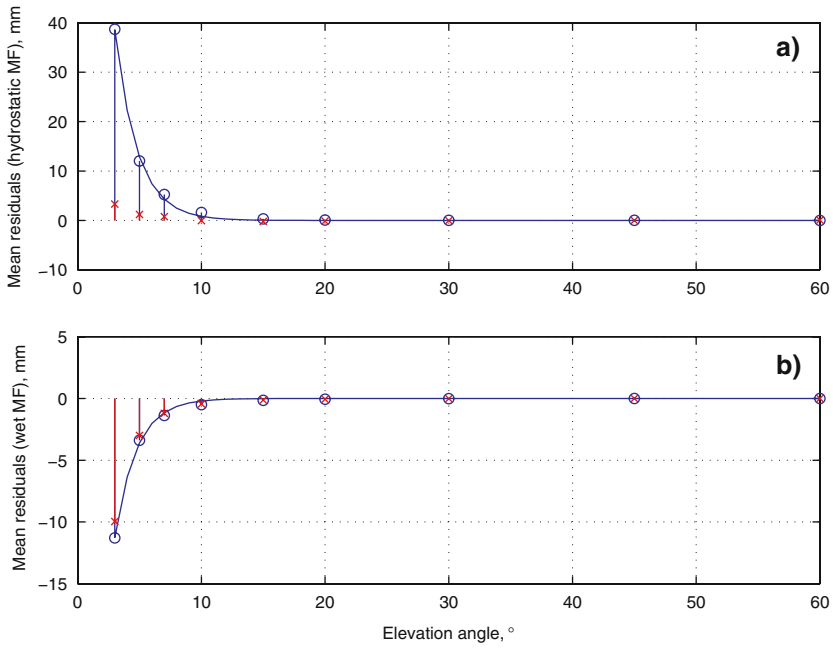

Fig. 7 Elevation angle dependence of the mean slant delay residuals for the NMFs (*circle*) and the IMFs (*cross*), calculated using radiosonde data for Landvetter (year 2000). The solid lines represent **a** an exponential model (Eq. 7) fitted to the mean residuals of the NMFh; **b** an exponential model fitted to the mean NMFw residuals for this location

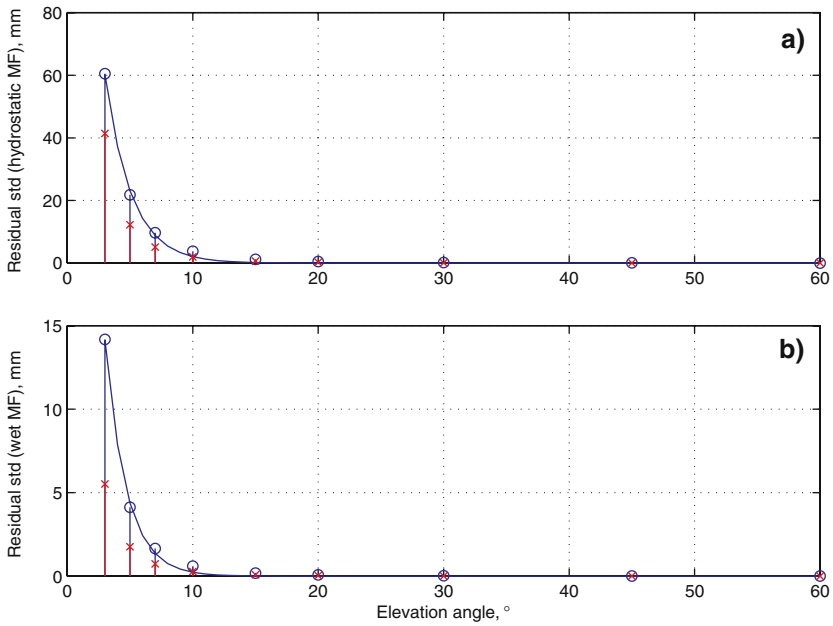

Fig. 8 Elevation angle dependence of the standard deviation of the slant delay residuals for the NMFs (*circle*) and the IMFs (*cross*). The *solid lines* represent **a** an exponential model (Eq. 8) fitted to the standard deviations of the NMFh residuals; **b** an exponential model fitted to the standard deviations of the NMFw residuals for Landvetter

However, the IMFw brings only a marginal improvement compared to the NMFw, in terms of mean and standard deviation of the residuals (presented by the crosses in Figs. 7b, 8b). We found that the IMFw errors remain correlated (correlation coefficient of about 0.99), for all studied pairs of elevation angles. Niell (2000) recognizes this and suggests using the simpler NMFw in combination with the IMFh.

4 Modeling of the mapping function residuals

4.1 Mean and standard deviation

The mean slant delay residuals due to the NMF/IMF, derived from ray tracing for the set of elevation angles discussed earlier, are plotted in Fig. 7. We adopt an exponential function as a model for the elevation dependence of the MF offsets, given by

$$\bar{m}(\varepsilon) = \bar{m}_0 \cdot \mathrm{e}^{-\varepsilon/\varepsilon_m}, \tag{7}$$

where the parameters $\bar{m}_0$ and ε_m are fitted in the least-squares sense to the mean residual data as shown in Fig. 7.

The standard deviation of the slant delay errors (Fig. 8) also can be modeled using an exponential function of the elevation angle:

$$\sigma(\varepsilon) = \sigma_0 \cdot \mathrm{e}^{-\varepsilon/\varepsilon_\sigma}. \tag{8}$$

The radiosonde data from the years 2000 and 2001 for the site at Landvetter yield the values presented in Table 1.

Table 1 Model parameters for the offsets and standard deviations of the slant delay residuals, derived from 2000–2001 radiosonde data for the site at Landvetter

Model parameter		Mapping function			
[unit]		NMFh	NMFw	IMFh	IMFw
Offset [m]	$\bar{m}_0$	0.170	−0.062	0.009	−0.048
Scale elevation (offset)	ε_m	1.8°	1.7°	2.3°	1.7°
Standard deviation [m]	σ_0	0.269	0.074	0.220	0.026
Scale elevation (std)	ε_σ	2.1°	1.7°	1.8°	1.9°
Decorrelation [days]	β^{-1}	5.35	0.56	3.30	2.91

4.2 Temporal behavior

Both the NMF and the IMF residuals remain time correlated after removing their systematic offset (recall Sect. 2.3). Assuming stationarity, the MF residuals can be modeled using a first-order autoregressive (Gauss–Markov) process of the form:

$$X(t_{k+1}) = \mathrm{e}^{-\beta\Delta t} X(t_k) + W(t_k)\,, \tag{9}$$

where the interval between the measurement instants t_k and t_{k+1} is denoted Δt, and $W(t_k)$ is a white Gaussian sequence. Such a process can be easily included in a Kalman filter procedure, as long as the parameter β is known (e.g., Brown and Hwang 1997).

The Gauss–Markov process with variance σ_X^2 has an exponential time-correlation function:

$$R_X(\tau) = \sigma_X^2 \cdot \mathrm{e}^{-\beta|\tau|}, \tag{10}$$

where τ is the time lag. The variance of the white sequence $W(t_k)$ can be expressed as $\sigma_W^2 = \sigma_X^2 \cdot (1 - e^{-2\beta\Delta t})$ when the Gauss–Markov process is uniformly sampled.

In our study, $X(t)$ represents the slant delay errors due to the MF imperfections. The values for β yielded by analysis of time correlations of the radiosonde ray-tracing residuals are summarized in Table 1, and will be used in the simulation study in the next section.

5 Impact study using simulations

5.1 Description of the simulation software

Our simulations are carried out using a Matlab-based Kalman filter imitating the setup of the GIPSY/OASIS-II processing software (Jarlemark et al. 2001; Webb and Zumberge 1993). At a given epoch, the linearity of the Kalman algorithm ensures that measurement perturbations affect the parameter estimates independently of the original measurements and estimates. We can therefore generate and study the effects of isolated measurement perturbations.

The standard setup of GIPSY/OASIS-II used for the geodetic GPS data processing at the Onsala processing center is characterized by:

- No satellite parameters are estimated, and the precise point positioning (PPP) method is used (Zumberge et al. 1997).
- State variables are updated at 5-min intervals.
- The unmodeled errors ν_Φ in Eq. (2) are assumed white and Gaussian, having standard deviations of 1 cm for all elevation angles.
- Estimation of the ZWD as a random walk process with a parameter $1.7 \times 10^{-4}\,\mathrm{m}/\sqrt{\mathrm{s}}$ and a site-specific a priori value for the ZHD.
- Estimation of the ZTD gradients (Davis et al. 1993) as random walk processes with a parameter $1.7 \times 10^{-5}\,\mathrm{m}/\sqrt{\mathrm{s}}$ (updated once per hour).
- Discrete fixed-interval smoothing (Rauch–Tung–Striebel smoothing) of the filter estimates (e.g., Brown and Hwang 1997).
- Elevation cut-off angle of 15°.

The above GIPSY/OASIS-II setup was reproduced in our simulation procedure with some modifications. Specifically, the elevation cut-off was varied between the simulation runs in order to study the impact of the MF errors. Random slant delay perturbations (the simulated MF errors) were subsequently applied according to the models described earlier. Due to the linearity of the Kalman filter, only these perturbations cause deviations between the different simulation runs. In the simulations, the Kalman iterations take place at 5-min intervals, and the perturbed final daily vertical coordinate is calculated when data from all 288 epochs are taken into account (i.e. a total period of 1 day).

At a fictitious GPS site at Landvetter, the average number of visible satellites is 7.4, 8.7, 9.6, and 10.1 for elevation cut-off angles of 15°, 10°, 7°, and 5°, respectively. Thus, 35% more measurements become available when 5° elevation cut-off is used instead of 15°, and the satellite geometry improves as more satellites become visible to the north.

5.2 Effects of the mapping bias

We simulated the impact of the elevation-dependent bias in the NMFs on the vertical coordinate estimate. The simulations were carried out using broadcast satellite ephemerides from the International GNSS Service (Beutler et al. 1999) for a fictitious site at Landvetter for 1 June 2000. The results are presented in Fig. 9 for cut-off angles at $\varepsilon = \{5, 7, 10, 15\}°$.

After the initial "convergence" in the forward run of the Kalman filter, the variations in the vertical coordinate are caused by the changing satellite constellation, which introduces varying weight to the mapping offset. The resulting offset in the vertical coordinate is negligible at 15° cut-off, and is ∼2.5 mm at 5° cut-off for the NMFs, dominated by the NMFh simulated errors.

A similar simulation was carried out for the IMFs, producing a smaller offset for the vertical coordinate of about −0.5 mm at 5° cut-off, and negligible offsets for larger cut-off angles. The negative sign of the result-

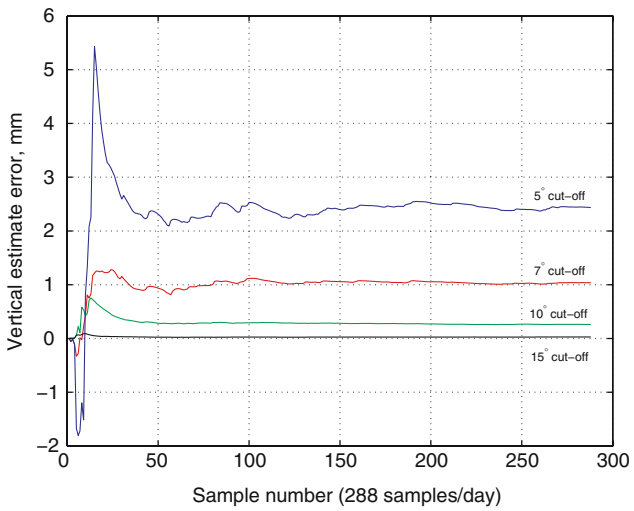

Fig. 9 Impact of the elevation-dependent offset in the NMFh/NMFw on the vertical coordinate estimate, for cut-off angles $\{5, 7, 10, 15\}°$

ing offset is due to the better performance of the IMFh compared to the NMFh, combined with the marginal improvement when using the IMFw instead of the NMFw (see Fig. 7).

5.3 Effects of the time-correlated mapping errors

We simulated the effects of the MF errors using an ensemble of 100 bias-free Gauss–Markov sequences (Eq. 9), and satellite constellations from a single day. We assumed azimuthal symmetry of the mapping errors. The weight given to the simulated mapping error depends on the GPS satellite constellation at that time, and the spread of the resulting ensemble of height estimates depends on the elevation cut-off angle. This simulation was carried out in order to study the uncertainty of the vertical coordinate estimate from one day to the next.

An example of ten sequences for 5° and 10° cut-off is shown in Fig. 10 for the NMFs with the Gauss–Markov process parameters presented in Table 1. The ensemble standard deviations at the end of the simulation runs were 3.2, 1.4 and 0.5 mm for cut-off angles 5°, 7° and 10°, respectively. The corresponding ensemble of simulation runs using the IMF error statistics (Table 1) yielded standard deviations of 2.0, 0.9, and 0.2 mm for elevation cut-off angles 5°, 7°, and 10°, respectively.

The longer-term effects of the MF errors were also evaluated by running the simulation software over 365 consecutive days. The behavior of the MF errors was constrained by the radiosonde measurements described in Sect. 3. These measurements give the initial and the final values of the simulated Gauss–Markov sequence and produce more realistic modeling of the MF errors for each day.

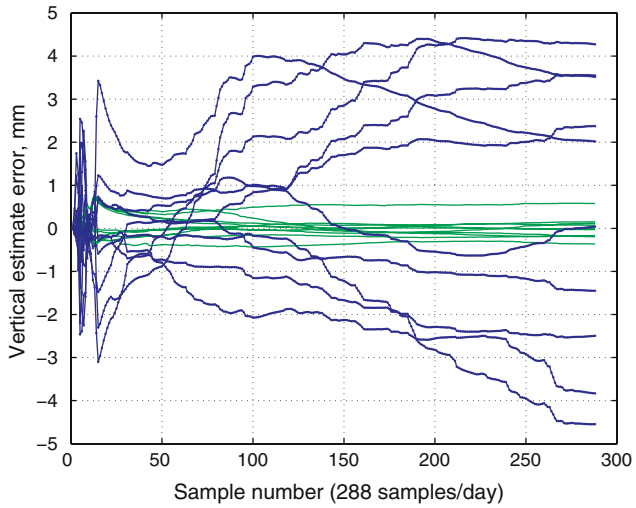

Fig. 10 Simulated impact of the combined NMF error variations affecting the estimated vertical coordinate, for cut-off angles 5° (*thick lines*) and 10° (*thin lines*). The NMF error variations were simulated using ensembles of Gauss–Markov sequences, each weighted according to the satellite elevations calculated from the GPS satellite ephemerides

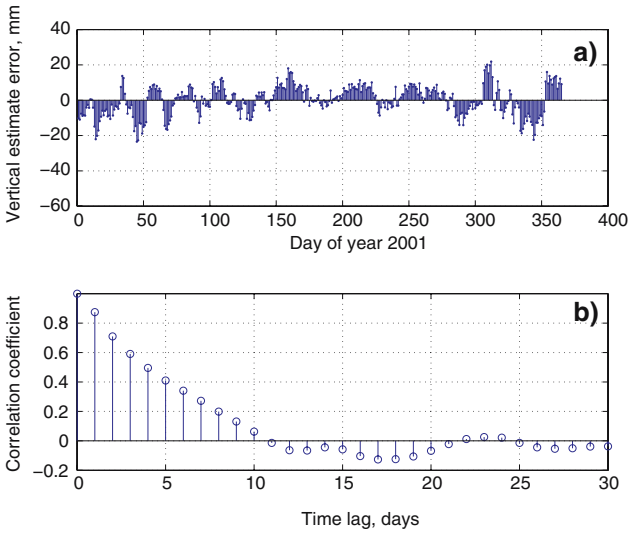

Fig. 11 **a** Simulated impact of the NMF error variations on the vertical coordinate estimate, for cut-off angle 5°. The MF error variations were approximated by a Gauss–Markov sequence, scaled according to the measurement elevation using Eq. (8), and fed into the simulation software in order to produce the vertical coordinate residuals. **b** Time correlations of the vertical component residuals above

Figure 11 presents simulation results at 5° cut-off, based on the NMF residuals obtained from ray-traced radiosonde data from 2001 at Landvetter. The standard deviation of these residuals is ∼8 mm, a value much larger than the corresponding ensemble standard deviation. This suggests that the vertical position errors due to mapping have a slowly varying (annual scale) component, and the lower graph in Fig. 11 shows a significant correlation over several days. The standard deviations of the NMF residuals for cut-off angles 7° and 10° were about 4 and 1 mm, respectively.

The corresponding standard deviation results for the IMF were about 4, 2, and 0 mm at 5°, 7°, and 10° cut-off respectively, and present a 50% improvement in comparison to the NMFs. In reality, one would expect somewhat larger variations due to the IMF errors, since the NWP model data used for the parameterization does not come from direct measurements at the GPS site.

6 Validation using geodetic GPS data

6.1 Time correlations of GPS height residuals

The temporal behavior of the errors in the GPS-estimated ZWD/ZTD can be studied indirectly, using the residuals of the vertical coordinate of a permanent

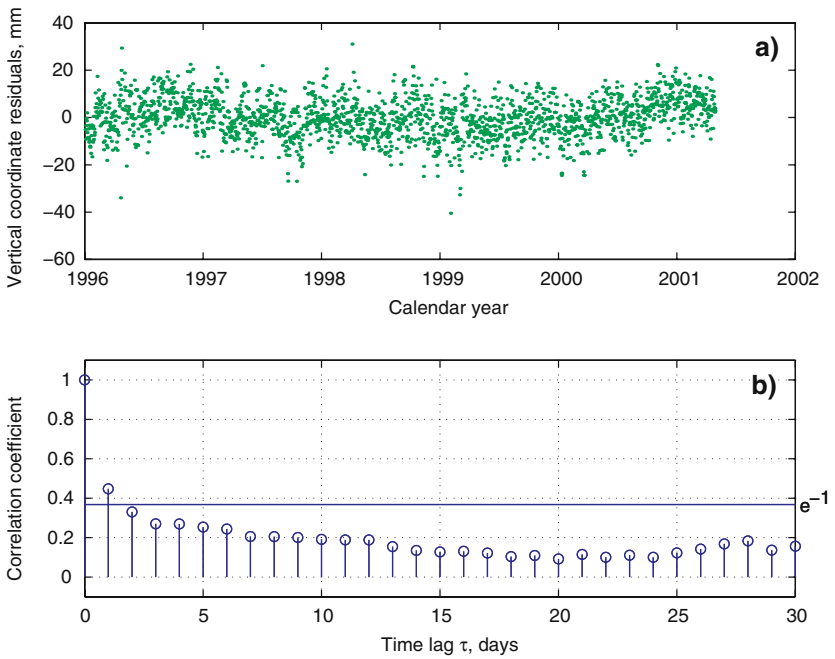

Fig. 12 **a** Time-series of the daily vertical coordinate residuals derived using GPS data from Onsala, Sweden; the respective temporal autocorrelation values are shown in graph **b**. The time correlation typically decreases to e^{-1} at a time lag $\tau \approx 2$ days

GPS site. This behavior depends on the data processing strategy, the MFs used, the antenna phase center modeling, and the modeling of the ocean/atmosphere loading effects.

Daily vertical coordinate estimates were calculated using GPS data from 1996 to the beginning of 2001 from regular "network" solutions obtained for a 15° elevation cut-off (Johansson et al. 2002). The daily estimates are based on 30-h measurements, and are used to deduce the vertical coordinate residuals after a correction for loading effects is applied (Scherneck et al. 2003). Time-series of these residuals are shown in Fig. 12, together with their temporal correlations.

The decrease in the temporal correlations of the height residuals is consistent for all sites in the SWEPOS Swedish geodetic GPS network in this data set (Scherneck et al. 2003). The decorrelation times for the residuals are about 1–2 days, and are summarized in Table 2. The standard deviations of the individual time-series were found to be less than 10 mm. Apparently, the northernmost sites have slightly longer decorrelation times and larger variability. This can be attributed to snow and ice accumulating on the antenna radomes during the winter (Jaldehag et al. 1996). Therefore, the presented vertical residual correlation times should be used as an approximation of the ZWD/ZTD error correlations cautiously, as the former correlations are larger than the latter.

The uncertainties of the vertical coordinate caused by the NMF errors at 15° elevation cut-off discussed earlier are well below the standard deviation values presented in Table 2. However, at low cut-off angles, the mapping errors become significant, and even with a proper description of the other elevation-dependent error sources (e.g., antenna radiation pattern and multipath effects), the use of cut-off angles smaller than 5° is not likely to improve the precision of geodetic GPS estimates of the vertical coordinate.

The time-series for the vertical coordinate have been corrected for linear trends, annual and sub-annual oscillations (up to three cycles per year), and air-pressure loading (Scherneck et al. 2003). However, there are unmodeled components on time-scales larger than 1 month, which cause the correlation estimates to remain rather high for time lags $\tau > 10$ days for some GPS sites, including the one at Onsala. In particular, the data for the years 1996 and 2000 appear to have positive trends (see Fig. 12a).

6.2 Time correlations of ZWD errors

In order to validate the relation between the errors in the ZWD and the vertical coordinate, we compared their temporal correlations using GPS data from Onsala, Sweden, and ZWDs measured by a WVR at the same location (e.g., Elgered and Jarlemark 1998). The multipath influence at this site is modest and well characterized (Granström 2006).

The GPS estimates of the ZWD are obtained from the ZTDs by removing the ZHDs calculated using surface pressure observations. We derived the temporal correlations for a 1-year time-series (year 2001) of differences between the WVR and GPS data at Onsala. As noted earlier, the errors due to the MFs are still present in these

Table 2 Decorrelation of the residuals of the vertical coordinates for the SWEPOS sites. The data sets span the years 1996–2001, and are produced by GIPSY/OASIS-II using a network solution. The temporal correlations are presented for time lag $\tau = 2$ days. The GPS sites are sorted by increasing latitude values, and their listed heights are above sea level

Site	Code	Lat. (°N)	Lon. (°E)	Height (m)	Corr. coeff. ($\tau = 2$ days)	St. dev. (mm)
Hässleholm	HASS	56.09	13.72	78.106	0.28	8.4
Oskarshamn	OSKA	57.06	16.00	120.890	0.30	8.5
Onsala	ONSA	57.40	11.93	9.559	0.33	8.4
Visby	VISB	57.65	18.37	54.848	0.34	8.4
Borås	BORA	57.72	12.89	185.397	0.32	7.7
Jönköping	JONK	57.74	14.06	228.431	0.28	7.9
Norrköping	NORR	58.59	16.25	13.980	0.30	8.0
Vänersborg	VANE	58.69	12.07	135.730	0.30	7.9
Lovö	LOVO	59.34	17.83	57.680	0.33	8.2
Karlstad	KARL	59.44	13.51	82.327	0.32	8.0
Mårtsbo	MART	60.59	17.26	50.437	0.36	8.3
Leksand	LEKS	60.72	14.88	448.148	0.35	8.7
Sveg	SVEG	62.02	14.70	459.244	0.35	8.2
Sundsvall	SUND	62.23	17.66	5.835	0.32	8.3
Östersund	OSTE	63.44	14.86	460.087	0.39	8.9
Umeå	UMEA	63.58	19.51	32.554	0.34	8.3
Vilhelmina	VILH	64.70	16.56	420.999	0.38	8.7
Skellefteå	SKEL	64.88	21.05	60.250	0.39	8.9
Överkalix	OVER	66.31	22.77	199.950	0.33	8.5
Arjeplog	ARJE	66.32	18.13	459.220	0.36	9.2
Kiruna	KIRU	67.88	21.06	469.055	0.40	10.0

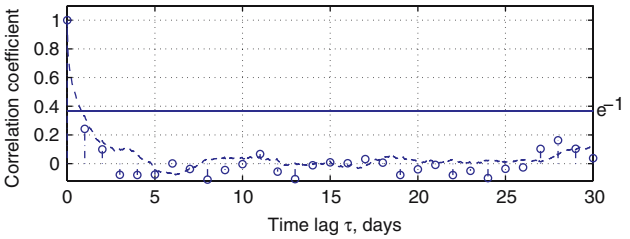

Fig. 13 Temporal correlation values for the vertical coordinate residuals from 2001 at Onsala (*circle*). The time correlations of the GPS–WVR differences in the ZWDs for 2001 are plotted for comparison (*dashed line*)

differences, but have a very small contribution because the cut-off angle has been set to 15°.

The correlation values decrease to e^{-1} at a time lag of about 1 day and are shown in Fig. 13. The agreement with the decorrelation time of the vertical residuals for this data set is notable. However, the temporal structure of the WVR errors is unknown; the time correlations of the GPS errors are masked and cannot be deduced from the GPS–WVR differences without reservations.

Simulations should be used in a future work to determine the combined effect of the known error sources on the temporal correlations of the GPS estimation errors. Comparing Figs. 12 and 13, we see that the vertical residual data from the early 2001 appear free of trends, explaining why the temporal correlations become negligible for $\tau > 1$ day.

7 Conclusions

We have determined the temporal correlations of the errors in the Ifadis MFs, NMFs, and IMFs. Their influence on the estimated vertical coordinate and the atmospheric delays has been addressed using simulations and data from a GPS receiver network in Sweden. The decorrelation times of the MF errors are of the order of 1 day for the NMFw and 3–4 days for the NMFh.

The contribution of the NMFh errors to the temporal correlations of the GPS height errors is greater, as the variability of the NMFh residuals is about five times larger than that of the NMFw residuals. The Ifadis MFh residuals exhibit a slowly varying offset, which causes the respective time correlations to remain high even on monthly scales. There is also a diurnal signature in these correlations, which makes the current use of the NMFs much more favorable.

The time correlations of the MF residuals for a given elevation angle are due to unmodeled variations of the atmospheric parameters. These correlations affect the GPS-estimated ZTDs in a complex way, since Eq. (4) is applied to measurements using satellites at various elevations, and ultimately depends on the chosen elevation cut-off angle. However, the presented effects of the time-correlated MF errors do not account for the contributions from mismodeled atmospheric delay gradients and turbulence.

The comparisons between the NMFs and IMFs show that the use of the latter reduces the resulting standard deviations of the estimation errors of the vertical component by half; a modest improvement for cut-off angles larger than 10°, where GPS data processing is normally carried out. The simulation results suggest that for cut-off angles below 10°, more accurate modeling of the atmospheric processes is needed, such as that shown in Figs. 7 and 8.

This improved modeling could involve additional state variables, and would take into account the means and the temporal correlations of the NMF errors. Correct modeling is also needed for the IMFs, since the variations and the time correlations of their errors are still significant at low elevation angles, although their bias is negligible. The choice of MFs will gain significance with the future refinement of the models for other error sources in GPS data processing.

This study is confined to the Swedish GPS network, making it specific to the area of Northern Europe. A similar analysis is needed for the improvement of the estimates produced by the geodetic GPS receiver networks exposed to different climate conditions. In the context of the assimilation of GPS data into NWP systems, a reliable description of the temporal correlations of the GPS estimation errors can be obtained using similar simulation methods, combining the known statistics of the individual GPS error sources.

Acknowledgments We are grateful to Alan Rogers, Jim Davis, Tom Herring, and Arthur Niell for providing the ray-tracing software. We acknowledge Lars Meuller at the Swedish Meteorological and Hydrological Institute for supplying the radiosonde data used in the analysis. This work was supported in part by the European Commission, through the Targeting Optimal Use of GPS Humidity Measurements in Meteorology (TOUGH) project in the Fifth Framework Programme (contract EVG1-CT-2002-00080), and by the Remote Sensing Committee of the Swedish National Space Board (contract 150/03). Our gratitude goes also to our reviewers for helping improve the quality of this article.

References

Bar-Sever YE, Kroger PM, Börjesson AJ (1998) Estimating horizontal gradients of tropospheric path delay with a single GPS receiver. J Geophys Res 103:5019–5035

Beutler G, Rothacher M, Schaer S, Springer TA, Kouba J, Neilan RE (1999) The International GPS service (IGS): an interdisciplinary service in support of earth sciences. Adv Space Res 23(4):631–635

Bisnath SB, Mendes VB, Langley RB (1997) Effects of tropospheric mapping functions on space geodetic data. In: Proceedings of the IGS Analysis Center Workshop, Jet Propulsion Laboratory, Pasadena, CA, pp 12–14 March

Brown RG, Hwang PYC (1997) Introduction to random signals and applied kalman filtering, 3rd edn. Wiley, New York

Crane RK (1976) Refraction effects in the neutral atmosphere. In: Meeks ML (ed) Methods of experimental physics, vol 12B. Academic Press, New York, pp 186–200

Daley R (1992) The effect of serially correlated observation and model error on atmospheric data assimilation. Mon Wea Rev 120(1):164–177

Davis JL, Herring TA, Shapiro II, Rogers AEE, Elgered G (1985) Geodesy by radio interferometry: effects of atmospheric modeling errors on estimates of baseline length. Radio Sci 20(6):1593–1607

Davis JL, Elgered G, Niell AE, Kuehn CE (1993) Ground-based measurement of gradients in the "wet" radio refractivity of air. Radio Sci 28(6):1003–1018

Elgered G, Jarlemark POJ (1998) Ground-based microwave radiometry and long term observations of atmospheric water vapor. Radio Sci 33(3):707–717

Granström C (2006) Site-dependent effects in high-accuracy applications of GNSS. Rep 13L, Department of Radio and Space Science, Chalmers University of Technology, Göteborg, Sweden

Herring TA (1992) Modeling atmospheric delays in the analysis of space geodetic data. In: De Munk J, Spoelstra TA (eds) Symposium on refraction of transatmospheric signals in geodesy. Netherlands Geodetic Commission, Delft, pp 157–164

Herring TA, Davis JL, Shapiro II (1990) Geodesy by radio interferometry: the application of Kalman filtering to the analysis of Very Long Baseline Interferometry data. J Geophys Res 95(B8):12561–12581

Ifadis I (1986) The atmospheric delay of radio waves: modeling the elevation dependence on a global scale. Rep 38L, School Electrical Computer Engineering, Chalmers University of Technology, Göteborg, ISBN: 99-0605353-4

Jaldehag RTK, Johansson JM, Davis JL, Elósegui P (1996) Geodesy using the Swedish permanent GPS network: effects of snow accumulation on estimates of site positions. Geophys Res Lett 23(13):1601–1604

Jarlemark P, Johansson J, Stoew B, Gradinarsky L, Elgered G (2001) Spatial error correlation of GPS atmospheres as determined from simulations. Phys Chem Earth 26(6–8):451–456

Johansson JM, Davis JL, Scherneck HG, Milne GA, Vermeer M, Mitrovica JX, Bennett RA, Jonsson B, Elgered G, Elósegui Koivula H, Poutanen M, Rönnäng BO, Shapiro II (2002) Continuous GPS measurements of postglacial adjustment in Fennoscandia. 1. Geodetic results. J Geophys Res 107(B8), 2157, Doi:10.1029/2001JB000400

MacMillan DS, Ma C (1994) Evaluation of very long baseline interferometry atmospheric modeling improvements. J Geophys Res 99(B1):637–651

Niell AE (1996) Global mapping functions for the atmosphere delay at radio wavelengths. J Geophys Res 101(B2):3227–3246

Niell AE (2000) Improved atmospheric mapping functions for VLBI and GPS. Earth Planets Space 52:699–702

Niell AE (2001) Preliminary evaluation of atmospheric mapping functions based on numerical weather models. Phys Chem Earth 26:475–480

Niell AE (2003) The IMF mapping functions. GPSMet Workshop, Tsukuba, Japan. Available from http://www.web.haystack.edu/geo/pubs/the_imf_mapping_functions_rev2.pdf

Niell AE, Coster AJ, Solheim FS, Mendes VB, Toor PC, Langley RB, Upham CA (2001) Comparison of measurements of atmospheric wet delay by Radiosonde, Water Vapor Radiometer, GPS, and VLBI. J Atmos Ocean Technol 18(6):830–850

Rocken C, Sokolovskiy S, Johnson JM, Hunt D (2001) Improved mapping of tropospheric delays. J Atmos Ocean Technol 18(7):1205–1213

Scherneck HG, Johansson JM, Koivula H, van Dam T, Davis JL (2003) Vertical crustal motion observed in the BIFROST project. J Geodyn 35:425–441

Webb FH, Zumberge JF (1993) An introduction to the GIPSY/OASIS-II. JPL Publ. D-11088, Jet Propulsion Laboratory, Pasadena, CA

Zumberge JF, Heflin MB, Jefferson DC, Watkins MM, Webb FH (1997) Precise point positioning for the efficient and robust analysis of GPS data from large networks. J Geophys Res 102(B3):5005–5017